06,13

Electrical conductivity and interface phenomena in thin-film heterostructures based on lithium niobate and lithium tantalate

© S.I. Gudkov[1], A.V. Solnyshkin[1], R.N. Zhukov[2], D.A. Kiselev[2], E.M. Semenova[1], A.N. Belov[3]

[1] Tver State University,
Tver, Russia
[2] National University of Science and Technology MISiS,
Moscow, Russia
[3] National Research University of Electronic Technology (MIET),
Zelenograd, Russia

E-mail: becauseimaphysicist@yandex.ru

Received January 18, 2023
Revised January 18, 2023
Accepted January 28, 2023

In this work, the electrophysical properties of metal-ferroelectric-semiconductor structures — $Cu/LiNbO_3/Si$ and $Ag/LiTaO_3/Si$ — with a ferroelectric layer thickness of 200 nm have been studied. The ferroelectric layers were deposited by RF magnetron sputtering. A topography study of thin film surface revealed a grain structure. The electrical conductivity mechanisms in $Cu/LiNbO_3/Si$ and $Ag/LiTaO_3/Si$ were considered. In a dependence of bias voltage value, there are a space charge-limited current, hopping conduction, and Schottky emission in $Cu/LiNbO_3/Si$ structures. For $Ag/LiTaO_3/Si$ structures, the space charge-limited current and hopping conduction were observed. An asymmetry of the current-voltage characteristics may indicate the presence of a potential barrier at the interface. For the studied structures, the value of the potential barrier was determined

Keywords: metal-ferroelectric-semiconductor structures, thin films, lithium niobate, lithium tantalate, electrophysical properties, electrical conductivity, potential barrier.

DOI: 10.21883/PSS.2023.04.55996.7

1. Introduction

Lithium niobate, ($LiNbO_3$ — LN) and lithium tantalate ($LiTaO_3$ — LT) are ferroelectric materials with ilmenite structure [1]. However, lithium tantalate with its higher melting temperature (about 1650°C for LT and about 1255°C for LN) and lower Curie temperature (about 600°C for LT and about 1050°C for LN) remains less investigated material than lithium niobate [1–3]. Currently, the most promising is the use of ferroelectric materials, in particular $LiNbO_3$ and $LiTaO_3$, not in the form of bulk crystals but in the form of thin-film structures applied on substrates. This is of relevance due to the possibility to use thin films in microelectromechanical systems, microelectronic devices and optical devices [4]. Thin films of lithium niobate and lithium tantalate can be used in thin-film waveguide optical modulators, in surface acoustic wave devices, in random access memory devices, in pyroelectric detectors, etc. [5,6]. The most common are metal–ferroelectric–semiconductor (MFeS) heterostructures based on thin films of ferroelectric materials. The study should take into account that their electrical and physical properties are affected by interface phenomena [7].

This study investigates topography of surface, electrical conductivity and barrier properties on interfaces of thin-film MFeS-heterostructures based on lithium niobate and lithium tantalate. It continues the investigations previously published in [8,9]. This study considers in detail the conduction mechanisms and determines magnitudes of the barriers.

2. Experimental part

Subjects of this study are thin-film metal–ferroelectric–semiconductor heterostructures based on lithium niobate and lithium tantalate. A thin ferroelectric layer was applied on (111)-oriented silicon substrates with *p*-type conductivity (*p*-Si) by RF magnetron sputtering in a SUNPLA-40TM vacuum chamber (the Republic of Korea). Before the application of the ferroelectric layer, the silicon substrates were cleaned by ion gun for 5 min.

LN samples were synthesized with a Z-cut $LiNbO_3$ plate as a target. The sputtering was conducted in the atmosphere of argon. Pressure was 0.5 Pa, magnetron power was 60 W. The post-growth annealing was performed in the air atmosphere at a temperature of 700°C for 120 min. Thickness of the LN layer was 200 nm. Copper round electrodes with a diameter of 2.45 ± 0.21 mm were applied on the free surface of the film. Thus, the samples have a MFeS-structure — $Cu/LiNbO_3/Si$.

LT samples were produced with a Z-cut $LiTaO_3$ plate as a target. The synthesis was carried out in the plasma of oxygen (40 vol%) and argon (60 vol%). Pressure was 0.57 Pa, magnetron power was 150 W. The post-growth annealing was performed twice in the air atmosphere: at a

temperature of 550°C for one hour and at a temperature of 700°C for one hour. Thickness of the $LiTaO_3$ layer was 200 nm. Silver round electrodes with a diameter of 4.5 ± 0.3 mm were applied on the free surface of the lithium tantalate film. The samples have a MFeS-structure — $Ag/LiTaO_3/Si$.

The surface of samples was investigated in the Laboratory of Magnetic Materials of the Scientific Instruments and Equipment Sharing Center of the Tver State University using a SolverNext scanning probe microscope (by „NT-MDT SI" LLC, the Russian Federation) in the mode of atomic-force microscopy (AFM). The dependence of current flowing through the structure on the applied bias voltage (current-voltage characteristics, IU-curves) was investigated using a E7-20 LCR meter (by „MNIPI" JSC, the Republic of Belarus) in the voltage range from -5 to 5 V. The voltage applied to the structure is considered as positive if positive potential is applied to the top electrode, and the voltage is considered negative in the case of reverse polarity. The experiment was conducted at room temperature.

3. Results and discussion

Images of thin film surfaces of LN and LT obtained with the use of AFM are shown in Fig. 1. It can be seen from Fig. 1, *a* that thin-film samples of LN have a grain structure. Diameter of grains varies in the interval from 100 to 300 nm. It can be seen from Fig. 1, *b*, that the surface of LT samples has a two-level structure. The top level is represented by grains with sizes of $3-4\,\mu$m. The bottom level (Fig. 1, *c*) has a grain structure with a mean roughness of up to 2.5 nm. Surface effects can influence electrical conductivity of the MFeS-structure.

Also, it is known [10], that conductive properties of thin dielectric films are strongly dependent on the film composition, its thickness, the level of energy and the density of traps. In most cases, current-voltage characteristics of MFeS-structures are complex. At low fields the density of current through the thin film is low and often can be described by the Ohm's law

$$J = \sigma E = q n_0 \mu \frac{V}{d}, \tag{1}$$

where J is current density, σ is electrical conductivity, E is electric field, q is elementary charge, n_0 is free carrier concentration in the state of thermal equilibrium, μ is electron mobility, V is applied bias voltage, d is film thickness.

As the strength of the external field increases, the conduction current becomes significant due to different conduction mechanisms [11]. According to [11], main conduction mechanisms in the metal–dielectric–semiconductor structure (MDS-structure) and, as a consequence, in the MFeS-structure include the following: Schottky emission, Fowler–Nordheim tunneling, direct tunneling, Pool–Frenkel emission, hopping conduction, space-charge-limited current (SCL-current). The key mechanism for a given voltage range can be determined by replotting IU-curves in the coordinates that allow identifying linear sections corresponding to a particular conduction mechanism.

Taking into account that this study investigates films with a thickness of 200 nm and that most often the direct tunneling is only possible in films with thicknesses less than $2-3$ nm and the Fowler–Nordheim tunneling is only possible in films with a thickness of an order of magnitude of several nanometers, these conduction mechanisms can be excluded from the consideration [12,13]. In [14,15] authors reported about the possibility to describe electric conductivity of lithium niobate films using the Ohm's law (at low fields), the Pool–Frenkel emission, the Schottky emission and the hopping conductivity.

Fig. 2 shows typical dependencies of current density on the bias voltage for thin films of lithium niobate (Fig. 2, *a*) and thin films of lithium tantalate (Fig. 2, *b*). The dependencies of J on V have a behavior of diode curves. IU-curves for thin films of lithium niobate and lithium tantalate have been discussed by us previously in [8,9].

Fig. 3 shows IU-curves of LN samples replotted in the coordinates that allow identifying the linear sections corresponding to a particular conduction mechanism. It can be seen from Fig. 3, *a*, that with the forward bias several linear sections are observed on the dependence of J on V on a logarithmic scale. Such behavior of the dependence of current density on the bias voltage is typical for the space-charge-limited current. If there are no traps, the SCL-current can be described by the following relation [11]:

$$J = \frac{9}{8} \mu \varepsilon_0 \varepsilon_s \frac{V^2}{d^3}, \tag{2}$$

where ε_0 is vacuum permittivity, ε_s is static permittivity. If there are traps, the following relationship is true:

$$J = \frac{9}{8} \mu \varepsilon_0 \varepsilon_s \theta \frac{V^2}{d^3}, \tag{3}$$

where θ is the ratio of free carrier density to density of total quantity of carriers. Within section I in Fig. 3, *a* the IU-curve follows the Ohm's law. The electrical conductivity calculated at low fields from the slope of straight line on the dependence of J on V (Fig. 2, *a*) is $\sim 1.02 \cdot 10^{-9}\,\Omega^{-1} \cdot \mathrm{m}^{-1}$; and value calculated at the intersection of the straight line (section I in Fig. 3, *a*) with the ordinate axis on the dependence of J on V on a logarithmic scale is $\sim 1.21 \cdot 10^{-9}\,\Omega^{-1} \cdot \mathrm{m}^{-1}$. In section II at a bias voltage from $V_T \approx 0.46$ V to $V_{TFL} \approx 0.78$ V a trap-limited space-charge conduction takes place. V_{TFL} voltage is the trap-filled limit voltage, after which a quick increase in the current density starts (section III). In section IV a trapless SCL-current is observed. With known trap-filled limit voltage V_{TFL}, the density of traps N_T can be determined from the following relationship [16]:

$$N_T = \frac{2\varepsilon_s \varepsilon_0 V_{TFL}}{q d^2}. \tag{4}$$

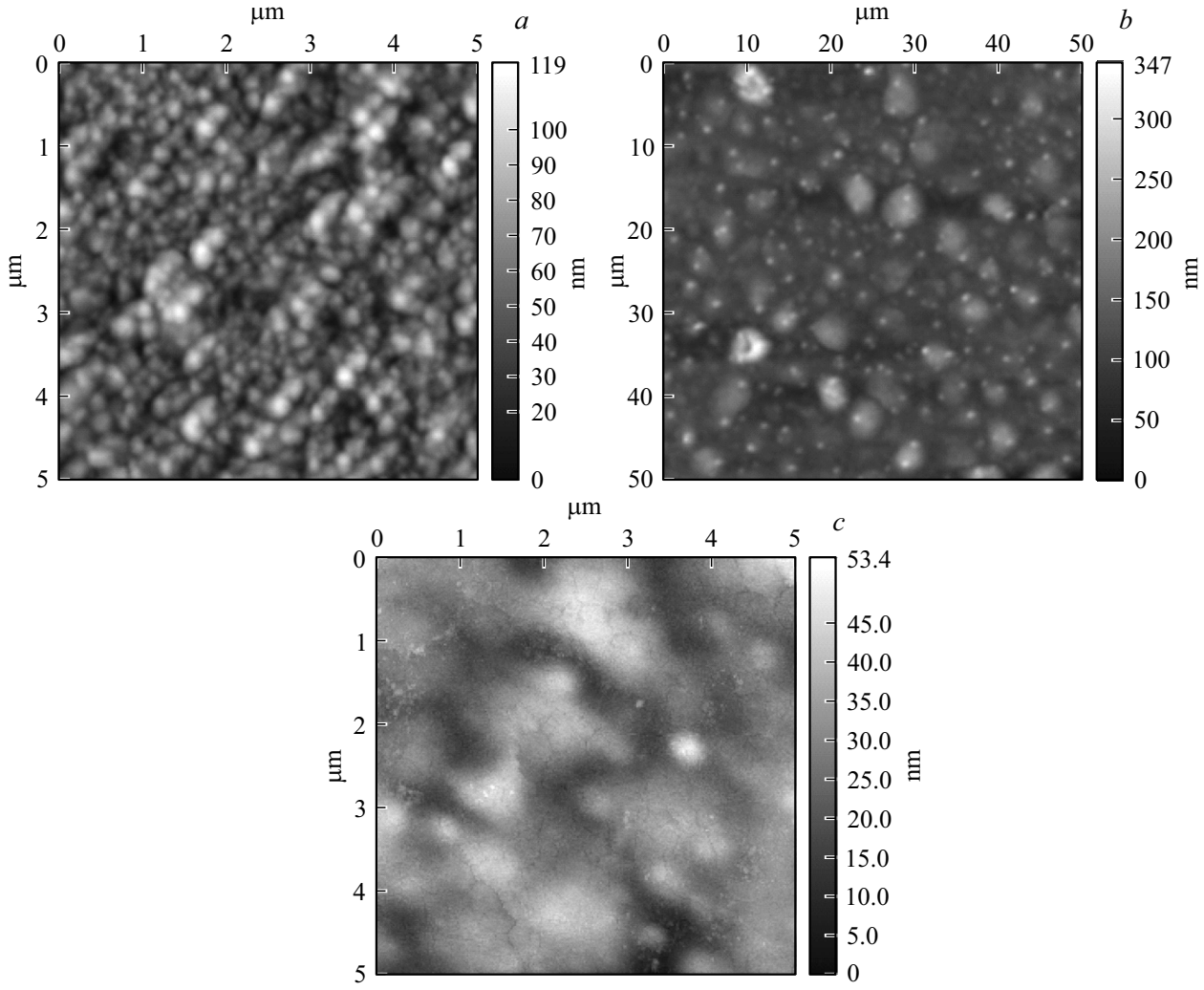

Figure 1. Topography of the surface obtained by the method of atomic-force microscopy for samples of lithium niobate (a) and lithium tantalate (b, c).

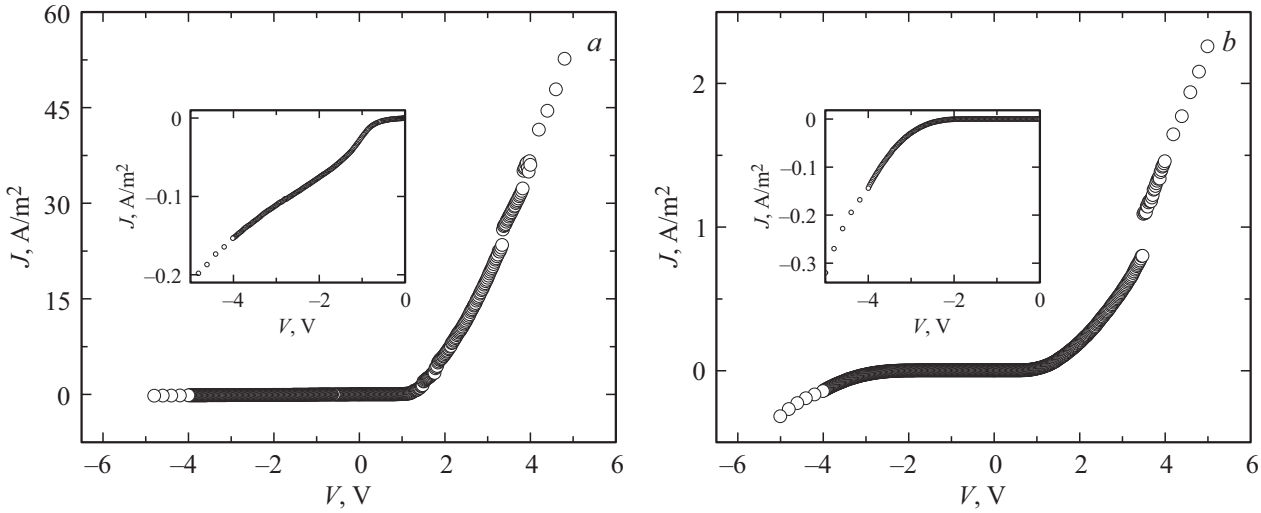

Figure 2. Current density as a function of bias voltage for thin films of lithium niobate (a) [8] and lithium tantalate (b) [9]. The inserts show scaled-up reverse bias.

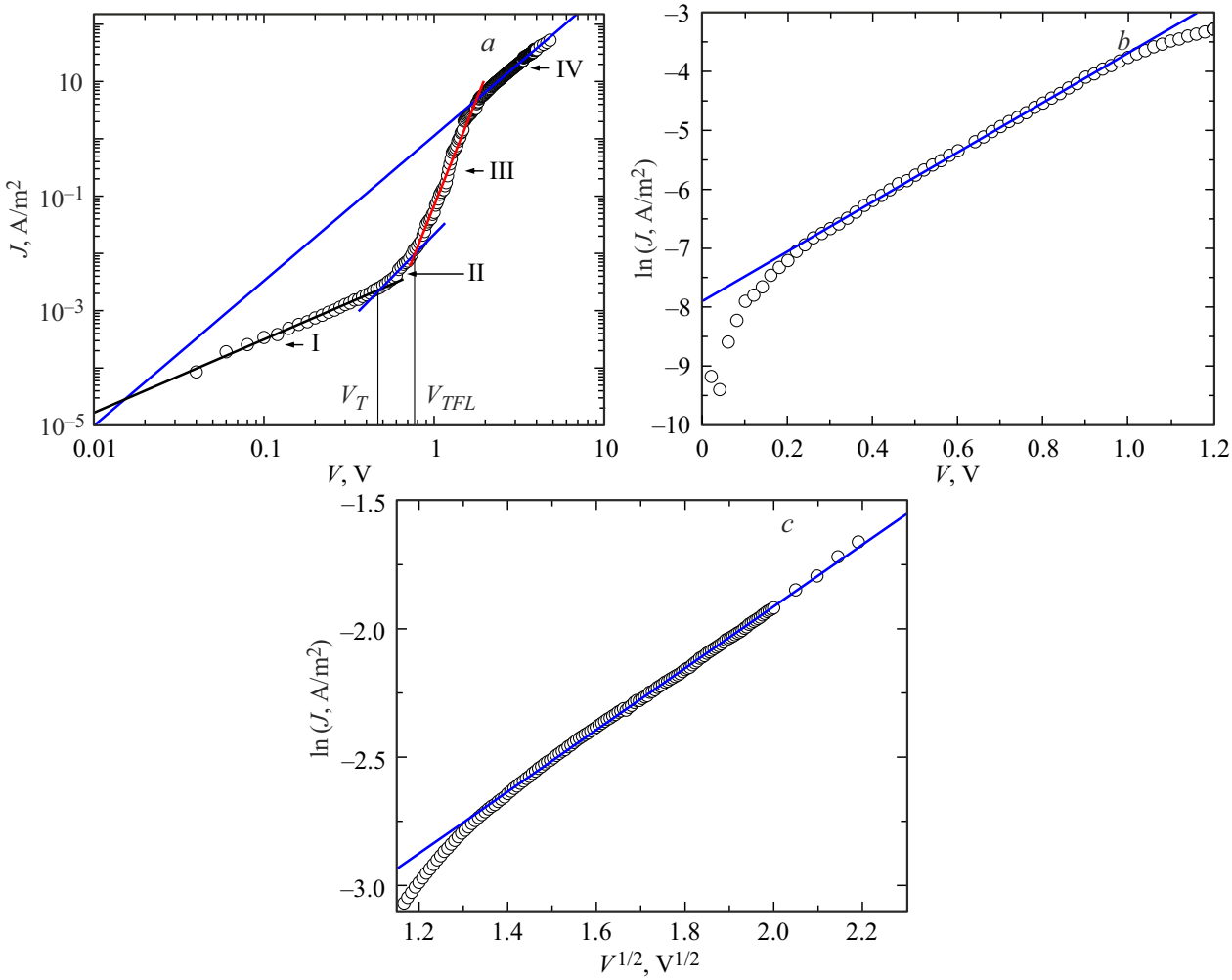

Figure 3. Current-voltage curves of the MFeS-structure based on lithium niobate with forward bias, which are typical for the SCL-current mechanism (a), as well as IU-curves with reverse bias, which are typical for the hopping conduction (b) and the Schottky emission (c). Straight lines are linear approximations.

Taking into account that $V_{TFL} \approx 0.78$ V, the density of traps is $\sim 9.55 \cdot 10^{22}$ m^{-3}. The ε_s for lithium niobate in the calculation was taken equal to ~ 44.29 [1].

With a reverse bias for the MFeS-structure based on $LiNbO_3$ the linear section on the dependence of J on V (Fig. 2, a) is observed in the range of voltages from 0 to 0.22 V, which is indicative of the fact the IU-curve follows the Ohm's law at these voltages. The electrical conductivity calculated from the slope of the straight line at this section is $\sim 0.79 \cdot 10^{-9}\ \Omega^{-1} \cdot$ m^{-1}. With increase in bias voltage above 0.22 V and up to 0.96 V, the linear section is observed in the dependence of $\ln J$ on V (Fig. 3, b), which is indicative of the fact that hopping conduction is the main mechanism here. The hopping conduction is described by the following relationship [11]:

$$J = qan_e\nu \exp\left[\frac{qaE}{kT} - \frac{E_a}{kT}\right], \qquad (5)$$

where a is mean hopping distance, n_e is electron concentration in the conduction band of the ferroelectric, ν is frequency of the thermal vibration of electrons at trap sites, k is the Boltzmann constant, T is absolute temperature, E_a is activation energy. According to (5), the slope of the straight line in the graph of $\ln J$ as a function of V can be used to calculate the mean hopping distance a, that corresponds to the mean spacing between trap sites. In our case: $a \approx 21.46$ nm. On the other hand, mean spacing between trap sites can be determined from the density of traps, taking into account that $a^3 = N_T^{-1}$ is the volume attributable to one trap. The a calculated in this way is ~ 21.88 nm, which is well consistent with the value determined from the slope of the straight line in the dependence of $\ln J$ on V. Further increase in the bias voltage results in transition to the Schottky emission. The expression for Schottky emission is as follows

$$J = A^* T^2 \exp\left[\frac{-q(\varphi_b - \sqrt{qE/4\pi\varepsilon_0\varepsilon_r})}{kT}\right], \qquad (6)$$

where $A^* = 4\pi qk^2 m^*/h^3$ is the effective Richardson constant, φ_b is the Schottky barrier height, ε_r is optical

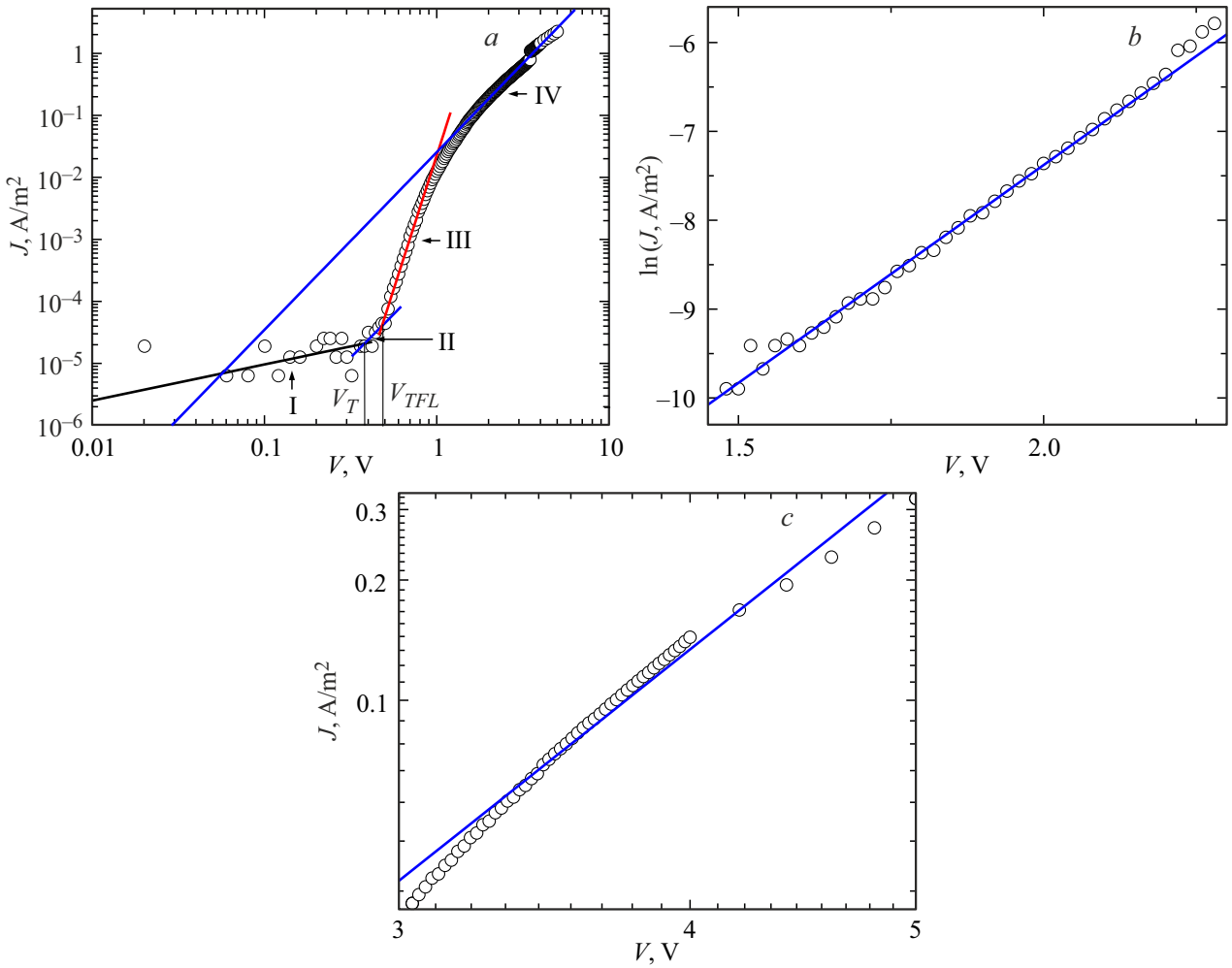

Figure 4. IU-curves of the MFeS-structure based on lithium tantalate with forward bias, which are typical for the SCL-current mechanism (a), as well as IU-curves with reverse bias, which are typical for the hopping conduction (b) and the SCL-current (c). Straight lines are linear approximations.

dielectric permittivity, m^* is effective electron mass in the ferroelectric, h is the Planck constant. The dependence of $\ln J$ on $V^{1/2}$ is linear in the case of Schottky emission. It is shown in Fig. 3, c. By formula (6), from the slope of the straight line in the dependence of $\ln J$ on $V^{1/2}$ the refraction index $n_r = \sqrt{\varepsilon_r}$ can be calculated. The calculation gave $n_r \approx 2.8$, which is well consistent with the values presented in literature: at a wavelength of $\sim 0.4-0.6\,\mu$m the refraction index of $LiNbO_3$ is $\sim 2.3-2.4$ [17,18].

Also, the prevailing conduction mechanisms were determined for MFeS-structures based on lithium tantalate, and IU-curves in appropriate coordinates are shown in Fig. 4. With the forward bias, the most probable is that the carrier transfer can be characterized by the space-charge-limited current. This is evidenced by several linear sections in the dependence of J on V on a logarithmic scale shown in Fig. 4, a. Section I in Fig. 4, a corresponds to the observance of the Ohm's law at voltages from 0 to $V_T \approx 0.38$ V. The electrical conductivity at this section is $\sim 4.87 \cdot 10^{-12}\,\Omega^{-1} \cdot \mathrm{m}^{-1}$ as determined from the slope of the straight line in the dependence of J on V (Fig. 2, b) and $\sim 7.34 \cdot 10^{-12}\,\Omega^{-1} \cdot \mathrm{m}^{-1}$ as determined from the intersection of the straight line with the ordinate axis in Fig. 4, a (section I). Section II in Fig. 4, a corresponds to the SCL-current with traps. The density of traps N_T for this structure calculated at $V_{TFL} \approx 0.50$ V by formula (4) is $\sim 5.89 \cdot 10^{22}\,\mathrm{m}^{-3}$ (ε_s for lithium tantalate was taken equal to ~ 42.60 [1]). Further increase in the bias voltage results in a sharp growth of the current density (section III) and transition to the trapless SCL-current (section IV).

With a reverse bias for the MFeS-structure based on $LiTaO_3$ the linear section corresponding to the Ohm's law in the dependence of J on V is observed up to the voltage of 1.46 V. The electrical conductivity determined for this section from the slope of the straight line in the dependence of J on V (Fig. 2, b) is $\sim 2.20 \cdot 10^{-12}\,\Omega^{-1} \cdot \mathrm{m}^{-1}$. In the voltage range from 1.48 to 2.20 V, hopping is the most probable conduction mechanism (Fig. 4, b). The mean spacing between trap sites calculated from the slope of the straight line in the dependence of $\ln J$ on V is ~ 24.93 nm;

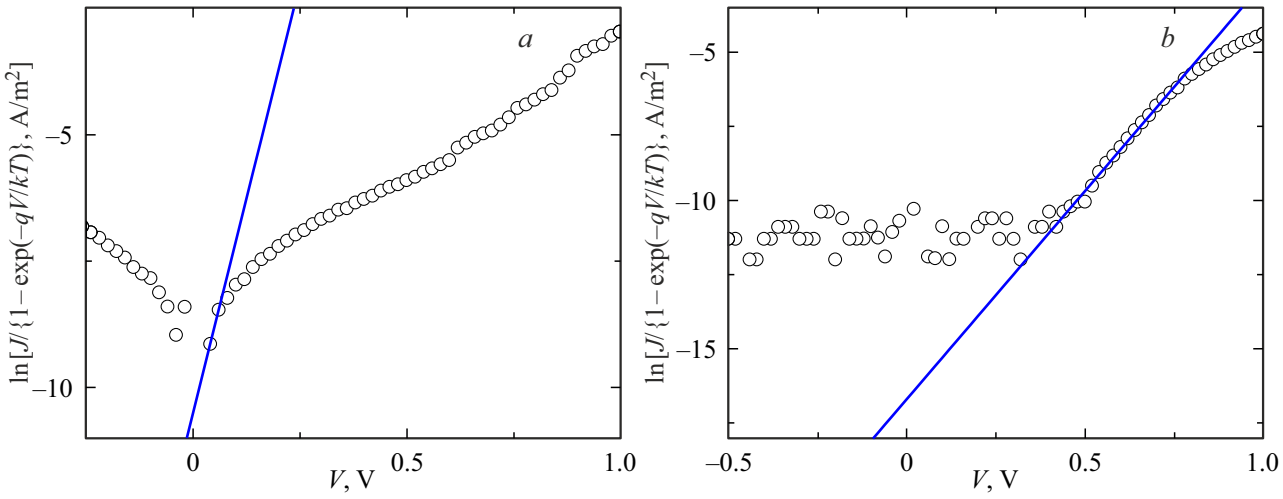

Figure 5. $\ln[J/\{1-\exp(-qV/kT)\}]$ as a function of V for thin films of lithium niobate (a) and lithium tantalate (b). Straight lines are linear approximations.

the a calculated with the use of trap density determined for the direct bias is ~ 25.71 nm. It is the most probable, that further increase in the reverse bias demonstrates a trend of transition to the space-charge-limited current (Fig. 4, c). And this current is not a trapless space-charge-limited current, because the slope coefficient of the straight line is $\alpha \approx 4.6$. This is indicative of the trap-limited current, which has the following dependence of current density on the bias voltage for the exponential distribution of traps over energies: $J \sim V^{\alpha}$, where $\alpha > 2$ and depends on the trap density [19,20].

One of characteristics of the film structure that has an effect on its electrical conductivity is the magnitude of the potential barrier arising at the interface. This parameter heeds to be accounted for when selecting a particular model to describe contact properties [21]. IU-curves shown in Fig. 2 are asymmetrical, which may be indicative of the presence of potential barrier at interfaces [22].

Magnitude of the potential barrier at an interface can be determined by the I–V-method [23–25]. This method has been applied for ferroelectric materials in [26]. With low bias voltages the current density J in Schottky diodes can be described as follows:

$$J = J_0\left[1-\exp\left(-\frac{qV}{kT}\right)\right]\exp\left(\frac{qV}{nkT}\right), \qquad (7)$$

where n is ideality factor (for the ideal diode $n = 1$, however, usually n is greater than unit), J_0 is saturation current density determined by the following relationship:

$$J_0 = A^* T^2 \exp\left(\frac{-q\varphi_e}{kT}\right), \qquad (8)$$

where φ_e is effective potential barrier height at a zero bias. φ_e can be calculated by formula (8)

$$\varphi_e = (\ln A^* T^2 - \ln J_0)\frac{kT}{q}. \qquad (9)$$

$\ln J_0$ is determined by the point of intersection of the ordinate axis and the straight line in the dependence of $\ln\left[J/\{1-\exp(-qV/kT)\}\right]$ on V with a direct bias. Also, from the slope of this straight line (slope coefficient is β) the ideality factor can be determined by the following formula:

$$n = \frac{q}{kT}\frac{1}{\beta}. \qquad (10)$$

Dependencies of $\ln[J/\{1-\exp(-qV/kT)\}]$ on V for the samples of LN and LT are shown in Fig. 5. To calculate the barrier height, values of the effective electron mass m^* were taken from [27]: for lithium niobate m^* was taken equal to $0.058m_0$, for lithium tantalate it was taken equal to $0.098m_0$, where m_0 being electron mass in vacuum. According to calculations, for a thin film of $LiNbO_3$ $\varphi_e \approx 0.84$ eV, $n \approx 1.16$, for a thin film of $LiTaO_3$ $\varphi_e \approx 1.01$ eV, $n \approx 2.81$. The high ideality factor for LT film may be due to additional effects related to the two-level structure of the film surface, grain boundaries and the influence of the series resistance [24].

Another method to determine the potential barrier height has been suggested in [28]. To describe the effect of the series resistance on the electrical conductivity, it is suggested to represent the Schottky diode as a diode and a R_s resistor connected in series [24,28]. In this case density of the current flowing through the structure is described as follows

$$J = J_0 \exp\left(\frac{q(V - SR_sJ)}{nkT}\right), \qquad (11)$$

where S is area of the electrode. It is easy to derive from this the following:

$$\frac{dV}{d(\ln J)} = SR_sJ + \frac{nkT}{q}. \qquad (12)$$

The dependence of $dV/d(\ln J)$ on J has a linear section at low bias voltages. Slope coefficient of the straight

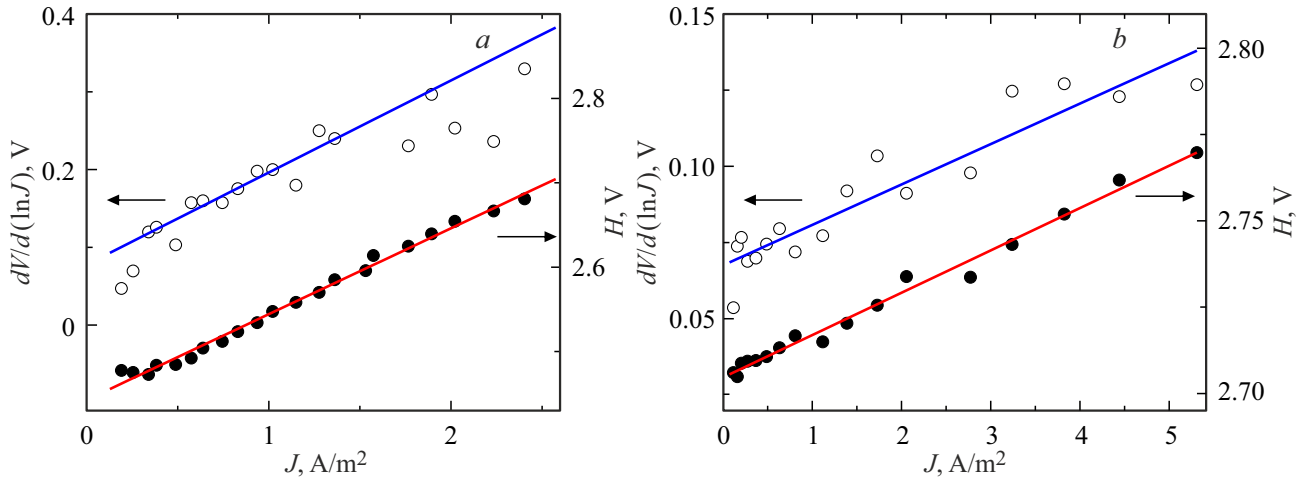

Figure 6. Dependencies of $dV/d(\ln J)$ and H on J for MFeS-structures based on lithium niobate (a) and lithium tantalate (b). Straight lines are linear approximations.

line approximating the linear dependence is SR_s, and the intersection with the ordinate axis takes place at $dV/d(\ln J) = nkT/q$. To determine the barrier height, the $H(J)$ function is considered:

$$H(J) = V - \frac{nkT}{q} \ln\left(\frac{J}{A^*T^2}\right). \quad (13)$$

On the other hand, according to [28]:

$$H(J) = SR_sJ + n\varphi_e. \quad (14)$$

The intersection between the straight line in the graph $H(J)$ and the ordinate axis gives $n\varphi_e$. By calculating n using relationship (12), the height of potential barrier can be determined. Also, the slope of the straight line in the graph of $H(J)$ allows determining the value of R_s and verifying the value obtained from (12). This method has been applied for ferroelectric materials in [29,30].

Dependencies of $dV/d(\ln J)$ and H on J for thin films of lithium niobate and lithium tantalate are shown in Fig. 6. For a lithium niobate thin film, the following values were obtained by this method: $n \approx 3.06$, $\varphi_e \approx 0.80$ eV; R_s from (12) is approximately equal to 25.19 MΩ, R_s from (14) is approximately equal to 21.65 MΩ. For a MFeS-structure based on lithium tantalate: $n \approx 2.66$, $\varphi_e \approx 1.02$ eV; R_s from (12) is approximately equal to 2.83 MΩ, R_s from (14) is approximately equal to 2.62 MΩ. Potential barriers determined by this method are well consistent with the values determined with the use of the dependence of $\ln[J/\{1 - \exp(-qV/kT)\}]$ on V.

Another way to determine R_s and φ_e has been suggested in [31]. To solve the problem of the series resistance, the following function is introduced

$$F(V) = \frac{V}{2} - \frac{kT}{q} \ln\left(\frac{J(V)}{A^*T^2}\right), \quad (15)$$

where $J(V)$ is current density as a function of bias voltage. The $F(V)$ dependence has a peak at a certain value of $V = V_0$. The potential barrier height can be determined from the following relationship:

$$\varphi_e = F(V_0) + \frac{V_0}{2} - \frac{kT}{q}. \quad (16)$$

The series resistance can be determined from the following relationship:

$$R_s = \frac{kT}{qJ_ZS}, \quad (17)$$

where J_Z is current density at V_0.

It can be seen, that this method does not allow determining of the ideality factor n. To determine n, it is necessary to use a modified version of this method [32]: a constant γ with an arbitrary value greater than n is introduced into the $F(V)$ function:

$$F(V, \gamma) = \frac{V}{\gamma} - \frac{kT}{q} \ln\left(\frac{J(V)}{A^*T^2}\right). \quad (18)$$

By setting two different values of γ, two systems of equations can be obtained

$$\varphi_{e1} = F(V_{01}, \gamma_1) + \left(\frac{1}{n} - \frac{1}{\gamma_1}\right)V_{01} - \frac{(\gamma_1 - n)kT}{nq}, \quad (19)$$

$$\varphi_{e2} = F(V_{02}, \gamma_2) + \left(\frac{1}{n} - \frac{1}{\gamma_2}\right)V_{02} - \frac{(\gamma_2 - n)kT}{nq} \quad (20)$$

and

$$R_{s1} = \frac{(\gamma_1 - n)kT}{qJ_{Z1}S}, \quad (21)$$

$$R_{s2} = \frac{(\gamma_2 - n)kT}{qJ_{Z2}S}. \quad (22)$$

By solving equations (19) and (20) together, the ideality factor can be determined:

$$n_V = \left(V_{01} - V_{02} + \frac{\gamma_2 kT}{q} - \frac{\gamma_1 kT}{q}\right) \Big/ \left(F(V_{02}, \gamma_2) - F(V_{01}, \gamma_1) - \frac{V_{02}}{\gamma_2} + \frac{V_{01}}{\gamma_1}\right), \quad (23)$$

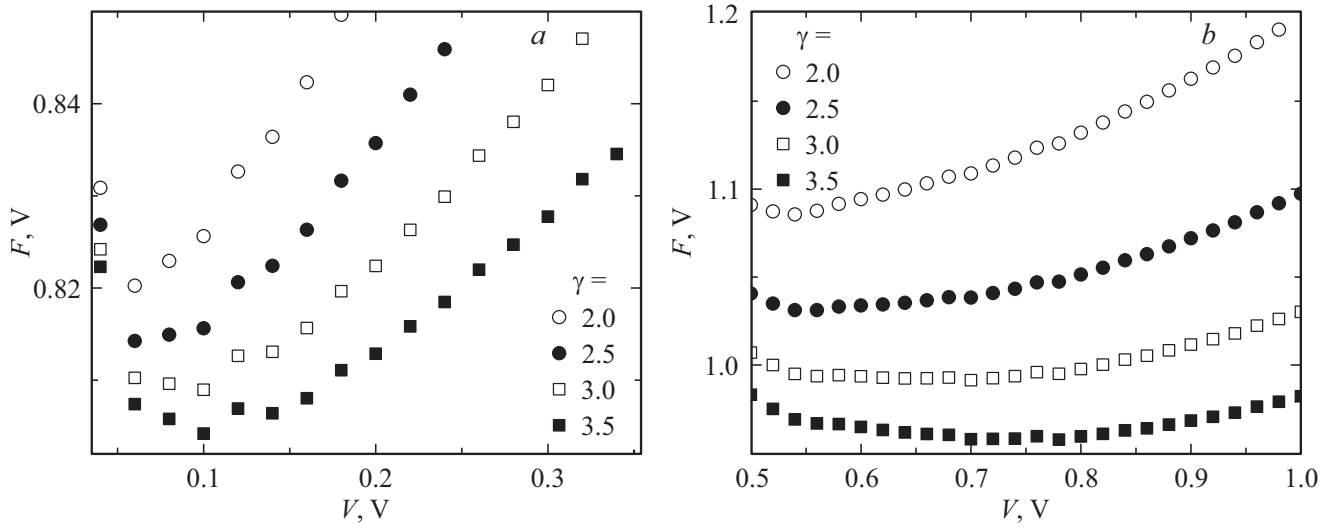

Figure 7. Dependencies $F(V, \gamma)$ at different values of γ for MFeS-structures based on lithium niobate (a) and lithium tantalate (b).

or n can be determined from (21) and (22):

$$n_J = \frac{\gamma_1 J_{Z2} - \gamma_2 J_{Z1}}{J_{Z2} - J_{Z1}}. \qquad (24)$$

Fig. 7 shows $F(V, \gamma)$ dependencies for the non-modified method ($\gamma = 2$) and for the modified method. By applying the non-modified method to heterostructures based on lithium niobate, we get $\varphi_e \approx 0.83$ eV, $R_s \approx 23.11$ MΩ, for heterostructures based on lithium tantalate we get $\varphi_e \approx 1.33$ eV, $R_s \approx 13.38$ MΩ. In the case of modified method γ was varied from 2.1 to 3.5. For the lithium niobate sample at different combinations of γ_1 and γ_2 values of φ_e fluctuate in the range from 0.81 to 0.82 eV; values of n_V vary from 1.17 to 2.56; values of n_J vary from 1.04 to 2.57. For $LiTaO_3$ at different combinations of γ_1 and γ_2 the φ_e has values in the range from 1.00 to 1.30 eV; values of n_V vary from 1.23 to 3.36; values of n_J vary from 1.11 to 3.33. Values determined by this method are consistent to the best extent with the data obtained by methods of [23,28]: at $\gamma_1 = 2.5$, $\gamma_2 = 3.1$ for $LiNbO_3$

$$\varphi_{e1}(n_V) \approx \varphi_{e2}(n_V) \approx \varphi_{e1}(n_J) \approx \varphi_{e2}(n_J) \approx 0.81\,\text{eV},$$

$$n_V \approx 1.69, \quad n_J \approx 1.73, \quad R_{s1}(n_V) \approx 22.83\,\text{MΩ},$$

$$R_{s2}(n_V) \approx 22.37\,\text{MΩ}, \quad R_{s1}(n_J) \approx R_{s2}(n_J) \approx 21.79\,\text{MΩ};$$

at $\gamma_1 = 2.8$, $\gamma_2 = 3.4$ for $LiTaO_3$

$$\varphi_{e1}(n_V) \approx \varphi_{e2}(n_V) \approx 1.02\,\text{eV},$$

$$\varphi_{e1}(n_J) \approx \varphi_{e2}(n_J) \approx 1.01\,\text{eV},$$

$$n_V \approx 2.55, \quad n_J \approx 2.70, \quad R_{s1}(n_V) \approx 2.44\,\text{MΩ},$$

$$R_{s2}(n_V) \approx 1.21\,\text{MΩ}, \quad R_{s1}(n_J) \approx R_{s2}(n_J) \approx 1.00\,\text{MΩ}.$$

To analyze current-voltage characteristics, let use consider the energy band diagram of the metal–ferroelectric–p-Si heterostructure shown in Fig. 8. This diagram was built in an assumption that prevailing charge carriers at low temperatures in lithium niobate and lithium tantalate are electron polarons [33,34].

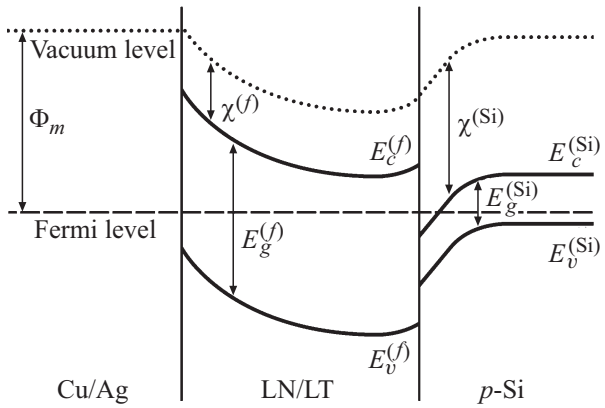

Figure 8. Energy band diagram of MFeS-structures under study: Φ_m is work function of the metal, χ is electron affinity, E_g is band gap, E_c is energy corresponding to the bottom of the conduction band, E_v is energy corresponding to the top of the valence band.

A barrier of Schottky type is formed at the metal–ferroelectric contact, which magnitude is determined by the work function of the metal, as well as by the electron affinity and positions of the Fermi level of the ferroelectric material. In the vicinity of the opposite surface the bending of bands in the ferroelectric from the side of the ferroelectric–p-Si heterojunction is due to the electron affinity of the materials and the position of Fermi level before the contact. At the contact, Fermi levels in the media are equalized and charge carriers are injected into the ferroelectric. The Fermi level in silicon crosses the bottom of the conduction band, and in the near-contact area silicon is a degenerate semiconductor of n–-type. Thus, the silicon substrate from the side of

ferroelectric material can be considered as a material with high electrical conductivity, which is close to conductivity of metals. Based on IU-curves, a conclusion can be made that the energy barrier height for charge carriers is mainly contributed from the metal–ferroelectric interface.

4. Conclusion

The topography of thin-film MFeS-heterostructures based on lithium niobate and lithium tantalate is investigated. It has been found that samples have a grain structure. The dependence of current flowing through the structure on the applied bias voltage is investigated. It has been found that IU-curves of MFeS-structures based on $LiNbO_3$ and $LiTaO_3$ follow the Ohm's law at low bias voltages. As the voltage increases, the most probable conduction mechanisms in thin films of lithium niobate are SCL-current for the forward bias and hopping conduction and Schottky emission for the reverse bias; in thin films of lithium tantalate the most probable conduction mechanisms are SCL-current for the forward bias and hopping conduction and SCL-current for the reverse bias. IU-curves demonstrate asymmetry, which may be indicative of the presence of potential barrier at the interfaces. By means of methods based on IU-curves, the barrier height is determined: for the LN thin film it is from 0.80 to 0.84 eV, for the LT thin film it is from 1.01 to 1.02 eV. Electrical conductive properties of the studied heterostructures are analyzed on the basis of energy band diagrams. It is shown that the observed effects are mainly contributed by the barrier at the metal–ferroelectric interface.

Funding

This study was supported by the Russian Science Foundation (grant No. 22-29-01102).

Conflict of interest

The authors declare that they have no conflict of interest.

References

[1] V.Ya. Shur. Lithium niobate and lithium tantalate-based piezoelectric materials. In: Advanced Piezoelectric Materials / Ed. Kenji Uchino. Woodhead Publishing, Cambridge (2010). P. 204. https://doi.org/10.1533/9781845699758.1.204
[2] A. Bartasyte, S. Margueron, T. Baron, S. Oliveri, P. Boulet. Adv. Mater. Interfaces **4**, *8*, 1600998 (2017). https://doi.org/10.1002/admi.201600998
[3] A.V. Yatsenko, M.N. Palatnikov, N.V. Sidorov, A.S. Pritulenko, S.V. Evdokimov. Phys. Solid State **57**, *8*, 1574 (2015). https://doi.org/10.1134/S1063783415050339
[4] A.R. Damodaran, J.C. Agar, S. Pandya, Z. Chen, L. Dedon, R. Xu, B. Apgar, S. Saremi, L.W. Martin. J. Phys.: Condens. Matter **28**, *26*, 263001 (2016). https://doi.org/10.1088/0953-8984/28/26/263001
[5] M.P. Sumets, V.A. Dybov, V.M. Ievlev. Inorg. Mater. **53**, *13*, 1361 (2017). https://doi.org/10.1134/S0020168517130015
[6] V. Stenger, M. Shnider, S. Sriram, D. Dooley, M. Stout. Proc. SPIE **8261**, Terahertz Technology and Applications V, 82610Q (2012). https://doi.org/10.1117/12.908523
[7] Z. Xi, J. Ruan, C. Li, C. Zheng, Z. Wen, J. Dai, A. Li, D. Wu. Nature Commun. **8**, *1*, 15217 (2017). https://doi.org/10.1038/ncomms15217
[8] S.I. Gudkov, K.D. Baklanova, M.V. Kamenshchikov, A.V. Solnyshkin, A.N. Belov. Phys. Solid State **60**, *4*, 743 (2018). https://doi.org/10.1134/S106378341804011X
[9] S.I. Gudkov, A.V. Solnyshkin, D.A. Kiselev, A.N. Belov. Cerâmica **66**, *379*, 291 (2020). https://doi.org/10.1590/0366-69132020663792885
[10] B.L. Yang, P.T. Lai, H. Wong. Microelectron. Reliab. **44**, *5*, 709 (2004). https://doi.org/10.1016/j.microrel.2004.01.013
[11] F.-C. Chiu. Adv. Mater. Sci. Eng. **2014**, 578168 (2014). https://doi.org/10.1155/2014/578168
[12] V. Mikhelashvili, G. Eisenstein. J. Appl. Phys. **89**, *6*, 3256 (2001). https://doi.org/10.1063/1.1349860
[13] E. Lim, R. Ismail. Electronics **4**, *3*, 586 (2015). https://doi.org/10.3390/electronics4030586
[14] V. Joshi, D. Roy, M.L. Mecartney. Integr. Ferroelectr. **6**, *1–4*, 321 (1995). https://doi.org/10.1080/10584589508019375
[15] N. Easwaran, C. Balasubramanian, S.A.K. Narayandass, D. Mangalaraj. Phys. Status Solidi A **129**, *2*, 443 (1992). https://doi.org/10.1002/pssa.2211290214
[16] F.-C. Chiu, H.-W. Chou, J.Y. Lee. J. Appl. Phys. **97**, *10*, 103503 (2005). https://doi.org/10.1063/1.1896435
[17] D.S. Smith, H.D. Riccius, R.P. Edwin. Opt. Commun. **17**, *3*, 332 (1976). https://doi.org/10.1016/0030-4018(76)90273-X
[18] D.F. Nelson, R.M. Mikulyak. J. Appl. Phys. **45**, *8*, 3688 (1974). https://doi.org/10.1063/1.1663839
[19] W. Brütting, S. Berleb, A.G. Mückl. Synth. Met. **122**, *1*, 99 (2001). https://doi.org/10.1016/S0379-6779(00)01342-4
[20] Y. Gu, L.J. Lauhon. Appl. Phys. Lett. **89**, *14*, 143102 (2006). https://doi.org/10.1063/1.2358316
[21] V.G. Bozhkov, N.A. Torkhov, A.V. Shmargunov. J. Appl. Phys. **109**, *7*, 073714 (2011). https://doi.org/10.1063/1.3561372
[22] V. Joshi, D. Roy, M.L. Mecartney. Appl. Phys. Lett. **63**, *10*, 1331 (1993). https://doi.org/10.1063/1.109721
[23] E.H. Rhoderick. Kontakt metall-poluprovodnik / eds. G.V. Stepanov, Radio i svyaz, M., (1982), 208 p. (in Russian).
[24] Z. Çaldíran, A.R. Deniz, Ş. Aydoğan, A. Yesildag, D. Ekinci. Superlattices Microstruct. **56**, 45 (2013). https://doi.org/10.1016/j.spmi.2012.12.004
[25] B. Akkal, Z. Benamara, B. Gruzza, L. Bideux. Vacuum **57**, *2*, 219 (2000). https://doi.org/10.1016/S0042-207X(00)00131-7
[26] D.Y. Wang. J. Am. Ceram. Soc. **77**, *4*, 897 (1994). https://doi.org/10.1111/j.1151-2916.1994.tb07245.x
[27] J. Yang, J. Long, L. Yang. Phys. B: Condens. Matter **425**, 12 (2013). https://doi.org/10.1016/j.physb.2013.05.017
[28] S.K. Cheung, N.W. Cheung. Appl. Phys. Lett. **49**, *2*, 85 (1986). https://doi.org/10.1063/1.97359
[29] P. Durmus, S. Altindal. Int. J. Mod. Phys. B **31**, *27*, 1750197 (2017). https://doi.org/10.1142/S0217979217501971
[30] A. Buyukbas-Ulusan, S. Altíndal-Yerişkin, A. Tataroğlu. J. Mater. Sci.: Mater. Electron. **29**, *19*, 16740 (2018). https://doi.org/10.1007/s10854-018-9767-8

[31] H. Norde. J. Appl. Phys. **50**, *7*, 5052 (1979). https://doi.org/10.1063/1.325607
[32] K.E. Bohlin. J. Appl. Phys. **60**, *3*, 1223 (1986). https://doi.org/10.1063/1.337372
[33] A.A. Esin, A.R. Akhmatkhanov, V.Ya. Shur. Ferroelectrics **496**, *1*, 102 (2016). https://doi.org/10.1080/00150193.2016.1157438
[34] A. El-Bachiri, F. Bennani, M. Bousselamti. Spectrosc. Lett. **47**, *5*, 374 (2014). https://doi.org/10.1080/00387010.2013.857356

Translated by Y.Alekseev